DOI: ADD DOINUMBER HERE

Structured H-infinity and Linear Parameter Varying Control Design for the VEGA Launch Vehicle

Diego Navarro-Tapia⋆*, Andrés Marcos*⋆*, Samir Bennani* ⋆⋆ *and Christophe Roux*⋆⋆⋆
⋆ *University of Bristol*
Bristol, BS8 1TR, United Kingdom (Technology for AeroSpace Control (TASC), www.tasc-group.com)
e-mail: diego.navarro-tapia/andres.marcos@bristol.ac.uk
⋆⋆ *ESA-ESTEC*
Noordwijk, 2201AZ, The Netherlands; e-mail: samir.bennani@esa.int
⋆⋆⋆ *ELV S.p.A.*
Colleferro, 00034, Italy; e-mail: christophe.roux@elv.it

Abstract

This article describes the application of two robust control design techniques: the structured $\mathcal{H}_\infty$ and the linear parameter varying (LPV) synthesis techniques to the design of the rigid-body atmospheric phase control system of a launch vehicle. The structured $\mathcal{H}_\infty$ synthesis technique allows to perform a robust $\mathcal{H}_\infty$-based design while keeping the same TVC controller architecture used by the launch vehicle. The LPV design approach can synthesize a scheduled controller by expressing the control problem in terms of time-varying parameters. The main goal is to explore the potentials for improvement by using a robust control design technique, which may reduce the tuning and design effort required for each mission, as well as, provide a more systematic and automated design approach. Both synthesis approaches are applied to the actual VEGA VV05 mission data. Finally, the two synthesized controllers are validated and compared with the VEGA baseline controller using a high-fidelity, nonlinear simulator.

1. Introduction

The design of the ascent-flight control system of a launch vehicle for the atmospheric phase is a challenging task. Along this first phase of the mission, any launch vehicle encounters undesired events such as wind disturbances, high aerodynamic pressure and rapid system dynamic changes. Further complications are introduced by the elastic behaviour of the launch vehicle, which may cause instability. In the face of all these adverse effects, the control system must satisfy very demanding and tight performance requirements and still be robust against a large range of substantial parameter dispersion.

In order to cope with the large dynamical system variations the control gains is typically scheduled along the flight trajectory using the so-called Gain Scheduling (GS) scheme.[20] It consists of linearising the vehicle around several representative points along the flight trajectory and designing a frozen time controller at each point. These individual controllers are then interpolated based on a parameter (e.g. time or non-gravitational-speed) resulting in a scheduled controller. This is the design approach used by the small European VEGA launcher, which uses a classical (proportional-derivative plus bending filters) controller for the Thrust Vector Control (TVC) system.[19]

This strategy has been proven successful for the nine missions VEGA has performed so far but several practical limitations are recognized. First, the GS strategy generally results in an expensive (in terms of both cost and time) design and validation process. Second, the classical framework only takes uncertainties in an implicit fashion using classical stability margins (gain and phase margins), and thus it must rely in a good analysis coverage (i.e. again costly and time intensive). Third, the performance and the robustness are not guaranteed for the flight instants between the design points of the scheduled controller. This feature is especially critical when the dynamics change rapidly between design points. And fourth, the tuning process is partially automated, with limited or no connection to other points or across missions.

In order to address these limitations, in this article, two robust control synthesis techniques are applied for the design of the VEGA launcher atmospheric phase control system: the structured $\mathcal{H}_\infty$ and the linear parameter varying (LPV) design techniques. Both approaches can reduce the tuning and design effort prior to each mission, as well as providing a more systematic design process approach.

On the one hand, the structured $\mathcal{H}_\infty$ approach allows to perform a $\mathcal{H}_\infty$-based design fixing the order and the structure of the controller. This technique has shown great promise and has led to intense study by the community, even resulting already in relevant Space flown missions, such as ESA Rosetta,[3] CNES Microscope,[18] and piloted flight tests.[14] In addition, this technique has also been successfully applied to launch vehicle control design in several investigations, using simulation models of different fidelity.[6,21]

On the other hand, the LPV synthesis technique offers several potentialities:[2]

1. the controller design and scheduling are incorporated to a single design procedure. This feature may reduce the tuning and design effort prior to each mission;
2. performance and robustness are guaranteed along the flight envelope;
3. it uses the same design framework as $\mathcal{H}_\infty$.

Despite the lack of powerful LPV software tools, this approach has also been applied to numerous works in aerospace applications[11,12] including launch vehicle control design.[5,24] However, the development of new software tools such as LPVTools[8] may facilitate and allow further advances in LPV theory.

This article extends the work done in references,[15,16] where the classical and robust control design frameworks are reconciled. In this paper, the main aim is to show the potential for improvement of the launcher design process by applying them to a high-fidelity, nonlinear model of the VEGA launcher. To do so, the VEGA baseline controller designed using the classical approach is compared with the structured $\mathcal{H}_\infty$ and LPV designs. This benchmarking is performed in terms of nonlinear Monte-Carlo time-domain simulations.

The layout of this paper is as follows: first, the VEGA launch vehicle and the rigid-body analytical model for the atmospheric phase are described in Section 2. Section 3 and Section 4 define the structured $\mathcal{H}_\infty$ and LPV control problem respectively. Those two sections also present the synthesis procedure for each design approach. Then in Section 5, the baseline controller, the structured $\mathcal{H}_\infty$ and LPV designs are compared and analysed in terms of nominal nonlinear time-domain responses but more importantly also for dispersed conditions through Monte-Carlo simulations. Finally, Section 6 ends with the conclusions.

2. VEGA launcher benchmark

2.1 VEGA launcher and mission

VEGA launcher is the new European Small Launch Vehicle developed under the responsibility of the European Space Agency (ESA) and European Launch Vehicle (ELV) as prime contractor. The launcher has successfully performed nine launches since February 2013.

VEGA follows a four-stage approach formed by three solid propellant motors (P80, Zefiro 23 and Zefiro 9) providing thrust for the 1st, 2nd and 3rd stages; and, a bi-propellant liquid engine (LPS) on the 4th stage. All stages are controlled using a TVC. There is also a Roll and Attitude Control System (RACS) performing 3-axes control during the ballistic phase and roll rate control during the propelled phases.

2.2 VEGA launcher model

The motion of the vehicle is described by the standard six-degree-of-freedom equations of motion, which account for the translational and rotational dynamics of the launch vehicle. The derivation of the equations of motion of a generic launch vehicle can be found in.[7] In this article, the dynamic model is built following reference,[17] where the equations of motion are expressed as a state-space model suitable for analysis and design. In addition, this formulation can also be used to further derive Linear Fractional Transformation (LFT) and Linear Parameter Varying (LPV) models. The extension to LFT is not covered in this article.

Due to axial symmetry of the vehicle about the roll axis, the design and analysis can be performed in a single plane, either the pitch or the yaw axis. This strategy is valid considering the roll rate negligible so the pitch and yaw axes can be assumed uncoupled and equal. In this work, the VEGA launch vehicle will be examined in the yaw plane.

As the design focus of this work is the rigid-motion, the flexible forces and moments can be disregarded in the design phase. Thus, the translational and rotational equations are expressed as the sum of forces and moments from rigid-body and nozzle motion dynamics, also known as the tail-wags-dog effect (see equations 1 and 2). In addition, other contributions such as rigid damping and wind disturbances are included. The design including the flexible-body dynamics will be addressed in future work.

$$m\ddot{z} = \Sigma F = F_r + F_n \tag{1}$$

$$J_{yy}\ddot{\psi} = \Sigma M = M_r + M_n \tag{2}$$

where m is the vehicle mass, J_{yy} is the moment of inertia, $\ddot{z}$ is the linear drift acceleration and $\ddot{\psi}$ the yaw attitude acceleration.

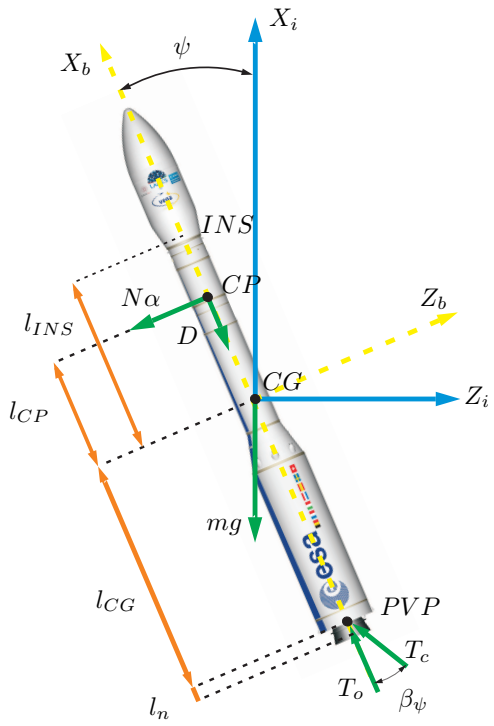

Figure 1: VEGA yaw-motion diagram

The rigid-body model in Figure 1 describes the vehicle motion due to thrust and aerodynamics. Using small-angle approximations, the rigid-body motion forces F_r and moments M_r are presented in equations 3 and 4 respectively.

$$F_r = -(T - D)\psi + N(\psi + \frac{\dot{z}}{V} + \frac{v_w}{V} - \frac{\dot{\psi}}{V}l_{CP}) - T_c\beta_\psi \tag{3}$$

$$M_r = Nl_{CP}(\psi + \frac{\dot{z}}{V} + \frac{v_w}{V} - \frac{\dot{\psi}}{V}l_{CP}) - T_c\beta_\psi l_{CG} \tag{4}$$

where T is the total thrust force, which is composed of the gimballed and ungimballed thrust forces, T_c and T_o respectively. D represents the aerodynamic drag force and N the aerodynamic normal force which is given by $N = QS_{ref}C_{N_\alpha}$, where Q is the dynamic pressure, S_{ref} is the launcher reference area and C_{N_α} is the lift gradient. l_{CP} is the distance from the center of gravity (CG) to the aerodynamic center of pressure (CP) and l_{CG} is the distance from CG to the nozzle pivot point (PVP). ψ is the yaw attitude angle, α is the angle of attack, β_ψ is the actuator deflection in the yaw plane, V is the launch vehicle speed, $\dot{z}$ is the vehicle lateral drift rate and v_w is the wind speed.

Similarly, the lateral force F_n and moment M_n due to the nozzle dynamics are given by:

$$F_n = -m_n l_n \ddot{\beta_\psi} \tag{5}$$

$$M_n = -(m_n l_n l_{CG} + I_n)\ddot{\beta_\psi} \tag{6}$$

where m_n is the nozzle mass, l_n is the distance from the nozzle center of gravity to the PVP. The moment of inertia of the nozzle engine about the PVP, I_n, is given by $I_n = I_o + m_n l_n^2$, where I_o is the moment of inertia of the nozzle engine about its center of gravity.

Finally, the sensed values are defined at the node location of the inertial navigation system (INS):

$$\psi_{INS} = \psi \tag{7}$$

$$z_{INS} = z - l_{INS}\psi \tag{8}$$

$$\dot{z}_{INS} = \dot{z} - l_{INS}\dot{\psi} \tag{9}$$

For analysis and design purposes, all the aforementioned relevant dynamics are generally expressed using a state-space formulation, as follows:

$$\begin{bmatrix} \dot{z} \\ \ddot{z} \\ \dot{\psi} \\ \ddot{\psi} \end{bmatrix} = \begin{bmatrix} 0 & 1 & 0 & 0 \\ 0 & a_1 & a_3 & a_2 \\ 0 & 0 & 0 & 1 \\ 0 & a_4 & a_6 & a_5 \end{bmatrix} \begin{bmatrix} z \\ \dot{z} \\ \psi \\ \dot{\psi} \end{bmatrix} + \begin{bmatrix} 0 & 0 & 0 \\ a_p & k_2 & -a_1 \\ 0 & 0 & 0 \\ k_1 & k_3 & -a_4 \end{bmatrix} \begin{bmatrix} \beta_\psi \\ \ddot{\beta}_\psi \\ v_w \end{bmatrix} \tag{10}$$

$$\begin{bmatrix} \psi_{INS} \\ z_{INS} \\ \dot{z}_{INS} \end{bmatrix} = \begin{bmatrix} 0 & 0 & 1 & 0 \\ 1 & 0 & -l_{INS} & 0 \\ 0 & 1 & 0 & -l_{INS} \end{bmatrix} \begin{bmatrix} z \\ \dot{z} \\ \psi \\ \dot{\psi} \end{bmatrix} + \begin{bmatrix} 0 & 0 & 0 \\ 0 & 0 & 0 \\ 0 & 0 & 0 \end{bmatrix} \begin{bmatrix} \beta_\psi \\ \ddot{\beta}_\psi \\ v_w \end{bmatrix} \tag{11}$$

The previous state-space model is composed of four rigid-body states (z,$\dot{z}$, ψ, $\dot{\psi}$); three inputs (β_ψ, $\ddot{\beta}_\psi$, v_w) and three outputs at the inertial navigation system (INS) position (ψ_{INS}, z_{INS}, $\dot{z}_{INS}$). The matrix coefficients are defined as:

$$\begin{aligned} &a_1 = \tfrac{-N}{mV}; && a_2 = -a_1 l_{CP}; && a_3 = \tfrac{-(T-D)}{m} + a_1 V; \\ &a_4 = \tfrac{N}{J_{yy}V} l_{CP}; && a_5 = -a_4 l_{CP}; && a_6 = a_4 V; \\ &k_1 = \tfrac{-T_c}{J_{yy}} l_{CG}; && a_p = -\tfrac{T_c}{m}; \\ &k_2 = -\tfrac{m_n}{m} l_n; && k_3 = \tfrac{-1}{J_{yy}}(m_n l_n l_{CG} + I_n); \end{aligned} \tag{12}$$

2.3 VEGA TVC controller

The VEGA TVC control architecture for each channel (pitch and yaw)[19] is based on a PD controller to stabilize the launcher's attitude, a lateral control feedback to reduce the angle of attack and to minimise the drift of the vehicle and a set of bending filters $H_\#$ (with $\# = 1 - 4$) to attenuate the bending modes (see Figure 2).

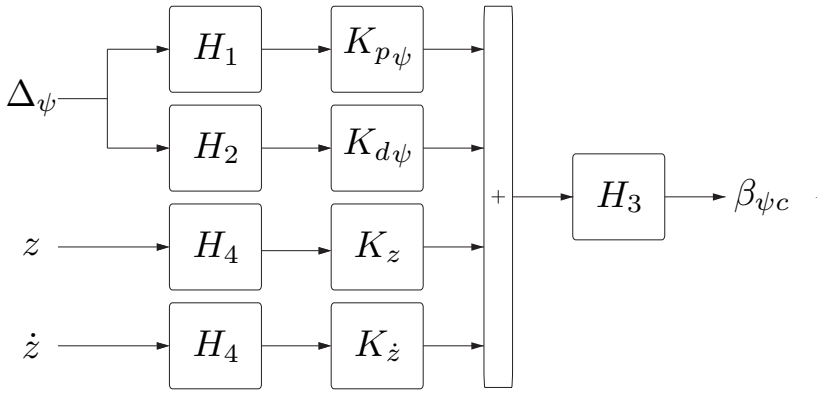

Figure 2: VEGA TVC Control Architecture

As mentioned in Section 1, the controller for the atmospheric phase is designed using a GS approach. First, a controller is design at every operational design point considering the launch vehicle model is a LTI model. Then, the controller gains and filters are scheduled based on some parameter (i.e. time, non-gravitational velocity, etc). Since in this work the flexible-body motion is not considered, the bending filters will not be implemented. The control law is defined in equation 13.

$$\beta_{\psi_c}(s,t) = \Delta_\psi(t)[K_{p_\psi}(t) + sK_{d\psi}(t)] + K_z(t)z(t) + K_{\dot{z}}(t)\dot{z}(t) \tag{13}$$

2.4 VEGA requirements

The TVC control system must satisfy very demanding stability and performance requirements. The most relevant specifications for the atmospheric phase are listed in Table 1.

	Requirements	Metrics	Bounds
Stability Requirements for nominal conditions	Rigid-body margins	LF-GM	$\geq$ 6 dB
		DM	$\geq$ 100 ms
		HF-GM	$\leq$ - 6 dB
Performance Requirements	Load Requirements	$Q\alpha$	$< Q\alpha$ envelope
	Lateral Control Requirements	z	$<$ 500 m
		$\dot{z}$	$<$ 15 m/s
	Actuation Requirements	β_ψ	$< 6.5^o$

Table 1: VEGA stability and performance requirements for the atmospheric phase

The stability requirements are based on the classical stability margins. In this case, only rigid-body margins are considered: low-frequency gain margin (LF-GM), delay margin (DM) and high-frequency gain margin (HF-GM). Those margins are assessed in the frequency domain through Nichols plots in a SISO approach (pitch and yaw channels are considered decoupled).[9] Since uncertainties are not considered in this work, only the stability requirements for nominal conditions are provided.

On the other hand, performance requirements must be verified via time-domain Monte-Carlo simulations using the nonlinear high-fidelity simulator VEGACONTROL. For further details on this simulator, the reader is referred to.[13] The different performance metrics must remain below given bounds in the face of parameter dispersion and disturbances such as noise and wind. The loads requirement is expressed as the product of the dynamic pressure and the angle of attack, $Q\alpha$ (see equation 14). To maintain the aerodynamic loads low, $Q\alpha$ must be below a given profile versus Mach.

$$Q\alpha = Q(\psi + \frac{\dot{z}}{V} - \frac{v_w}{V}) \tag{14}$$

Furthermore, the lateral displacement with respect to the reference trajectory frame shall be limited in the atmospheric phase (both in position z and velocity $\dot{z}$). Note that load alleviation and lateral control are opposite strategies, since the load alleviation will change the launcher trajectory to reduce the aerodynamic loads on the vehicle. Thus, a trade-off between both goals must be done. Finally, the actuator effort shall be also limited to avoid saturation and reduce TVC consumption.

3. Structured $\mathcal{H}_\infty$ design

This section describes the design of the VEGA atmospheric phase control system using the structured $\mathcal{H}_\infty$ synthesis technique. Firstly, the design framework is introduced and explained in detail. Then, guidelines for the weighting function selection are provided and finally the linear structured $\mathcal{H}_\infty$ controllers are briefly described.

3.1 Problem formulation

The design model used in this work is based on the closed-loop shown in Figure 3. Note that the real system has only one command, the yaw attitude command ψ_c. The drift and drift-rate commands, z_c and $\dot{z}_c$ respectively, are added to account for the interactions between the attitude and the lateral control channels in the design. In addition, a noise input has been implemented to model sensor errors. The diagram blocks K, G_τ, G_{TVC}, G_{wind} and G_{LV} are described below.

The closed-loop used for design consists of four main blocks:

1. Launch vehicle model (G_{LV})
   This block represents the model described in Section 2.2.

2. Controller (K)
   The controller K is based on the TVC controller structure described in Section 2.3, which is of the form:

$$K = [K_{p_\psi} + \frac{s}{T_f s + 1} K_{d\psi} \quad K_z \quad K_{\dot{z}}] \tag{15}$$

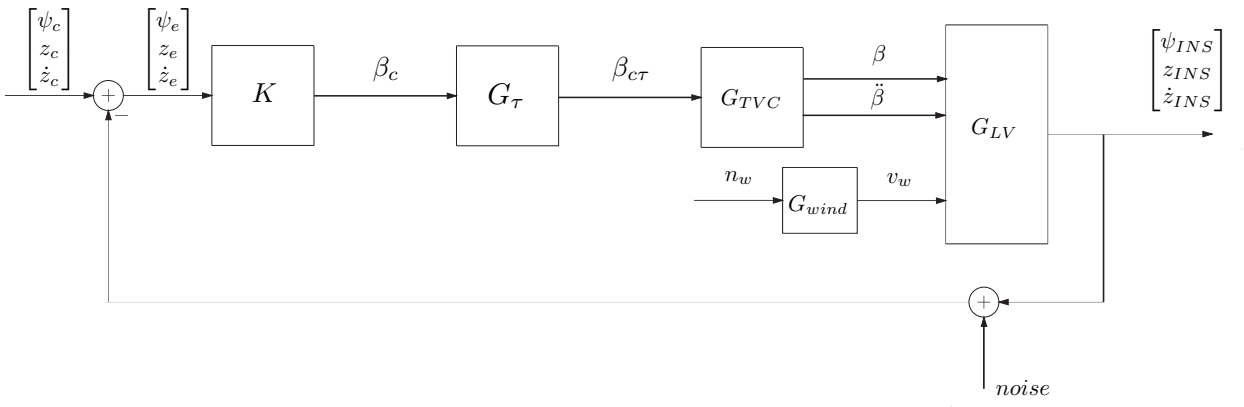

Figure 3: Closed-loop diagram for design

The controller structure defined in equation 15 does not include the set of filters H. It should be remarked that for ease of design the derivative filter H_2, which performs a derivative action, has been replaced by a first-order filter. Note that the pseudo-derivative term T_f has been fixed and therefore will not be tuned. This allows to focus the optimisation on the rigid-body controller gains: K_{p_ψ}, K_{d_ψ}, K_z and $K_{\dot{z}}$.

3. TVC actuator (G_{TVC})
   This model is derived to fit the actuator dynamics obtained from hardware-in-the-loop simulations. The acceleration of the actuator deflection $\ddot{\beta}_\psi$ is also included to account for nozzle dynamics. The details of this model can be found in reference.[22]

4. Delay (G_τ)
   The delay originated by the digital processing of the on-board computers and the actuators is modelled by a 2^{nd} order Padé approximation. In this work, a delay of 39 ms is implemented.

5. Wind generator (G_{wind})
   For an adequate design it is key to introduce wind models that represent the wind profiles that the launcher will encounter in the real flight. In this study, following the criteria found in,[1] the wind disturbance input is modelled by coloring white noise n_w through a Dryden filter with the following frequency response function:

$$G_{wind}(s,h) = \frac{v_w}{n_w} = \frac{\sqrt{\frac{2}{\pi}\frac{V(h)-v_{wp}(h)}{L(h)}\sigma^2(h)}}{s + \frac{V(h)-v_{wp}(h)}{L(h)}} \tag{16}$$

   where the values of the turbulence length scales $L(h)$ and standard deviations $\sigma(h)$ are given in tables in *Andrews*[1] for light, moderate and severe turbulence versus altitude.

   Finally, the build-up wind speed profile envelope $v_{wp}(h)$ is described in equation 17. This envelope is defined for the first 20 Km of altitude, which is the altitude range where the wind disturbance plays a significant role in performance indicators such as $Q\alpha$ (see equation 14).

$$v_{wp}(h) = \begin{cases} 10A[(\frac{h}{H_l})^{0.9} - 0.9\frac{h}{H_l}] & \text{for} \quad 0 \le h < H_l \\ A & \text{for} \quad H_l \le h \le H_f - H_u \\ \frac{A}{2}[1 - cos(\frac{\pi}{H_u}(h - H_f))] & \text{for} \quad H_f - H_u < h \le H_f \end{cases} \tag{17}$$

   where H_f = 20000 m, H_l = 2000 m, H_u = 2500 m and A = 14 m/s.

   The dryden filter G_{wind} combined with the planar steady-state profile v_{wp} defined in equation 17 are able to cover the wind estimated from VEGA VV05 flight data.[22] Therefore, unlike the classical control design approach where the wind disturbance are not considered in the design, this wind generator allows to perform the design accounting for real wind profiles.

All the blocks in Figure 3, except for the controller, can be assimilated into a single global augmented plant P, with commands, wind disturbance and noise channel as exogenous inputs. The output signals of P have been chosen to cope with all the requirements presented in table 1.

The next step in the approach is to define the control problem formulation. The structured $\mathcal{H}_\infty$ design framework offers new design capabilities such as the multi-channel formulation,[4] where instead of considering the global augmented plant, it is possible to define constraints to a set of closed-loop transfer functions. Since the optimisation can be performed over certain selected channels, this new feature may simplify the design process. However, this approach may overlook the contribution of some relevant channels of the system. In this work, the control problem is expressed as a standard $\mathcal{H}_\infty$ formulation as shown in Figure 4. This formulation allows to consider the full closed-loop system, accounting for all the interactions between channels.

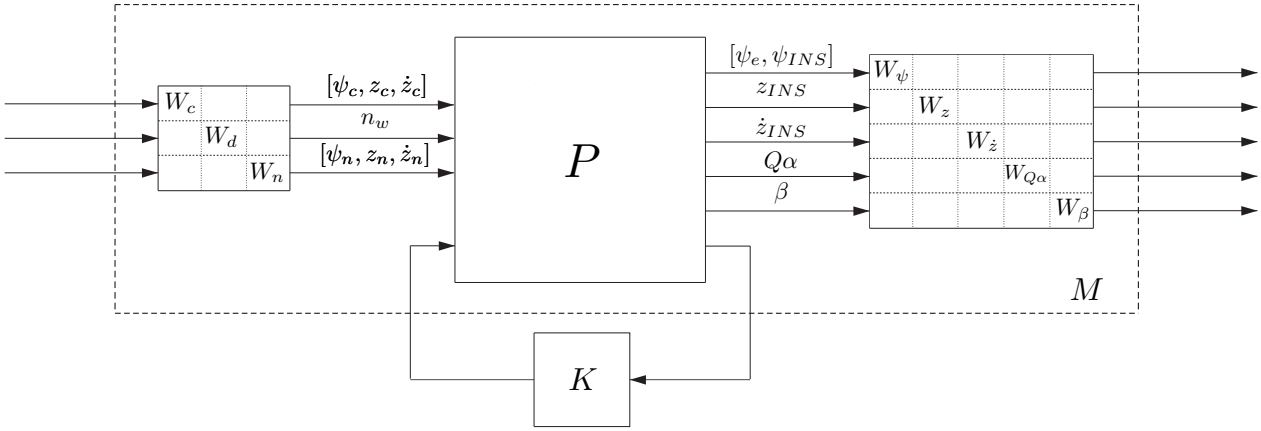

Figure 4: Standard $\mathcal{H}_\infty$ interconnection

The structured $\mathcal{H}_\infty$ optimisation consists of finding the controller K which minimises the $\mathcal{H}_\infty$ norm of the cost function in equation 18. This optimisation process is implemented in MATLAB through the command *hinfstruct*.

$$\min_K \|\mathcal{F}_l(M, K)\|_\infty \tag{18}$$

where $\mathcal{F}_l$ denotes the lower Linear Fractional Transformation (LFT), M is the augmented closed-loop (including the weighting functions) and K is the tunable structured controller.

The objective of the controller is to ensure stability throughout the flight while satisfying the requirements listed in Table 1. Furthermore, the controller must minimize the contribution from wind disturbance. The design objectives are introduced through input and output weighting functions scaling P (see Figure 4). Tracking objectives and stability requirements are imposed on the attitude channel by W_ψ. Similarly, the weights W_z and $W_{\dot{z}}$ address the lateral control objectives while $W_{Q\alpha}$ adds constraints to satisfy the load requirements. Finally, the actuation performance is limited by W_β.

3.2 Weighting function selection

In this section, the specific weighting functions used for the VEGA VV05 structured $\mathcal{H}_\infty$ design are described. In this work, the design uses the developed interconnection and weight setup as the one in reference,[16] but differs in the value of the weights in order to improve the design. Similarly, the weights are directly related to physical properties of the launch vehicle and specifications. This approach facilitates the understanding of how the system requirements are imposed on the weighting functions.

Proper scaling of the input and output variables is key for a good control design, particularly working with multiple-input multiple-output (MIMO) systems. It is also important to use the same units at both sides to improve the conditioning of the design problem. In this work, all scaled variables representing angles are expressed in degrees.

Unlike $\mathcal{H}_\infty$ synthesis, in which the order of the weighting functions is generally conserved low to avoid high-order designs, when using the fixed-order $\mathcal{H}_\infty$ synthesis there is no restriction on the order of the weights. Nevertheless, for ease of tuning and to facilitate the design process, constant and first order weighting functions are used.

The input weighting functions are chosen to scale the closed-loop dynamics at the input side with respect to their expected variation. The commanded input scaling matrix W_c considers a maximum attitude angle command ψ_c of 1 degree. Furthermore, W_{zc} and $W_{\dot{z}c}$ are defined to scale the lateral control channels. Thus, the input reference weight is given by:

$$W_c = \begin{bmatrix} W_{\psi_c} & 0 & 0 \\ 0 & W_{z_c} & 0 \\ 0 & 0 & W_{\dot{z}_c} \end{bmatrix} = \begin{bmatrix} \pi/180 & 0 & 0 \\ 0 & 5 & 0 \\ 0 & 0 & 1.5 \end{bmatrix} \tag{19}$$

The input disturbance weight W_d defines the normal distribution of the unitary white noise input n_w of the wind generator (see Figure 3). In this work, in order to minimize the wind disturbance contribution in the system, severe turbulence is considered to build the wind model. Using this configuration, one standard deviation was found to be sufficient. This ensures that approximately 68 % of the severe wind levels will be consider in the Gaussian process described by the Dryden filter G_{wind}. Then, W_d is given by:

$$W_d = 1 \tag{20}$$

The input noise weight W_n presented in equation 21 models the sensor noise of each feedback measurement. Firstly, a noise level of 0.02 degree is expected from the IMU sensor used by VEGA. For the lateral deviation measurements, the estimated noise levels provided by the guidance module are estimated to be around 0.01 meters for the drift and 0.001 meters/second for the drift-rate.

$$W_n = \begin{bmatrix} W_{\psi_n} & 0 & 0 \\ 0 & W_{z_n} & 0 \\ 0 & 0 & W_{\dot{z}_n} \end{bmatrix} = \begin{bmatrix} 0.02\frac{\pi}{180} & 0 & 0 \\ 0 & 0.01 & 0 \\ 0 & 0 & 0.001 \end{bmatrix} \tag{21}$$

The output weighting functions impose the system requirements on the design optimisation. Furthermore, they also scale the closed-loop dynamics at the output side (similarly, all the output angle variables are expressed in degrees). As mentioned in the introduction, in order to facilitate the understanding of the design, the weighting functions must be connected with system requirements and based on the expected output values of the controlled variables. Then, the weight selection becomes an iterative process in which the weights are tuned to obtain a good controller.

W_ψ establishes the tracking objectives and stability requirements in equation 24. ${W_\psi}^{-1}$ bounds the classical sensitivity and complementary sensitivity functions of the yaw attitude channel, i.e. ψ_e and ψ_{INS} respectively. On the one hand, ψ_e is limited by ${W_{\psi_e}}^{-1}$, which is defined as a constant weighting function of 3 dB. This constraint assures good stability margins since the peak of the sensitivity function directly yields a lower bound on the classical stability gain margin (GM) and phase margin (PM) through the following relations[23] :

$$GM \geq \frac{\|S(j\omega)\|_\infty}{\|S(j\omega)\|_\infty - 1} \tag{22}$$

$$PM \geq 2\arcsin\Big(\frac{1}{2\|S(j\omega)\|_\infty}\Big) \tag{23}$$

On the other hand, ψ_{INS} is weighted by ${W_{\psi_{INS}}}^{-1}$, which is a low-pass filter that limits the closed-loop bandwidth. This bandwidth should be sufficiently high to have an adequate tracking but low enough to avoid interactions with the first bending mode. ${W_{\psi_{INS}}}^{-1}$ presents a low-frequency gain around 10dB, a high-frequency gain of -80dB to force the roll-off at high frequencies and a crossover frequency of 10 rad/s.

$$W_\psi = \frac{\pi}{180}\begin{bmatrix} W_{\psi_e} & 0 \\ 0 & W_{\psi_{INS}} \end{bmatrix} = \frac{\pi}{180}\begin{bmatrix} 0.71 & 0 \\ 0 & \frac{s+3.162}{0.0001s+10} \end{bmatrix} \tag{24}$$

W_z and $W_{\dot{z}}$ enforce the lateral control requirements on the design process. ${W_z}^{-1}$ and ${W_{\dot{z}}}^{-1}$ shall correspond to the maximum drift and drift rate output expected values. For this design, in order to improve the lateral deviation performance tighter constraints than the ones used to recover the VEGA baseline controller in reference[16] are applied. Thus, a constraint of 20m drift is defined (see equation 25) and a maximum drift rate of 2m/s (see equation 26).

$$W_z = 1/20 \tag{25}$$

$$W_{\dot{z}} = 1/2 \tag{26}$$

The load requirements are set through the weighting function $W_{Q\alpha}$. In this case, the inverse of $W_{Q\alpha}$ puts a constraint of 2 degrees on the angle of attack α, ensuring that $Q\alpha$ is maintained below the safety envelope. $W_{Q\alpha}$ is given by:

$$W_{Q\alpha} = \frac{\pi}{180}Q\frac{1}{2} \tag{27}$$

Finally, W_β imposes the actuation requirements. Similarly, ${W_\beta}^{-1}$ shall refer to the maximum actuator deflection, which is 6.5 deg. However, as it is remarked in reference,[16] the VEGA baseline controller presents much higher components at high frequencies. Thus, a factor of approximately 2 is applied to the maximum deflection, resulting in the following constant weighting function:

$$W_\beta = \frac{\pi}{180}\frac{1}{12.5} \tag{28}$$

Although not implemented in this work, it should be mentioned that other requirements, such as actuation rate or angular acceleration, can also be considered in the design.

3.3 Structured $\mathcal{H}_\infty$ linear point designs

The structured $\mathcal{H}_\infty$ design is carried out at several operational points along the atmospheric phase. 8 structured $\mathcal{H}_\infty$ designs were performed under nominal conditions, one for each flight instant between t=20s and t=90s in intervals of 10 seconds. Note that this interval does not cover events such as lift off (approx t=4s) and tail-off separation (approx t=97s), which have different controller structure and requirements.

The same set of weighting functions described in subsection 3.2 are applied for all the design points. The 8 structured $\mathcal{H}_\infty$ controllers has the same controller structure as the baseline (see equation 15). The $\mathcal{H}_\infty$-norm obtained by these linear designs are in the range between 1.7 and 2.7. This variability in gamma can be reduced by using different weighting functions for each linear design point. However, for the scope of this paper this gamma range is not an issue. Thus, a simpler approach using the same weighting functions was performed, favouring also a simpler comparison with the LPV design technique (see Section 4).

4. Linear parameter varying design

This section describes the design of the VEGA atmospheric phase control system using the LPV synthesis technique. First, the LPV modelling process and the LPV control problem formulation are introduced. Finally, the LPV synthesized controller is briefly described.

4.1 LPV modelling

First, the VEGA launcher model is formulated as a LPV model. As the name indicates, LPV systems are linear systems which are dependent on a set of time-varying parameters $\theta(t)$. The LPV state space description is formulated as follows:

$$\dot{x}(t) = A[\theta(t)]x(t) + B[\theta(t)]u(t) \tag{29}$$

$$y(t) = C[\theta(t)]x(t) + D[\theta(t)]u(t) \tag{30}$$

The time variation of $\theta(t)$ is assumed to be unknown but measurable in real time. Therefore, variables such as dynamic pressure or angle of attack, which are generally not well estimated, should not be considered. In this article, time has been chosen as a scheduling variable for ease of simplicity. Future works will consider other time-varying parameters such as the non-gravitational velocity (VNG), which is the one implemented in VEGA to perform gain scheduling.[19]

For the LPV modelling, a grid-based approach has been used,[10] which consists of forming the LPV model from a set of linearised systems. This LPV modelling technique is conceptually represented in Figure 5. The LPV VEGA model employed in this work is built using the MATLAB toolbox LPVTools recently developed by MUSYN Inc.[8] This toolbox provides the necessary data structures and functions for modelling, simulation, analysis and design of LPV systems. In this work, the LPV VEGA model $G_{LV}(\theta)$ is constructed based on a grid of 8 linearised models from t=20s to t=90s in intervals of 10 seconds with time as a scheduling parameter.

To validate the LPV modelling, the bode plot of the attitude channel for the LPV and LTI models are compared in Figure 6 for two different flight instants: one that corresponds to a grid point, t=30s, and t=65s which is located between two linearisation points. At each grid point, the LPV model is described by the respective LTI model at that point. Thus at t=30s, there are no differences between both frequency responses (see left plot in Figure 6). At flight instants between the 8 linearisation points, the system is linearly interpolated. At t=65s, because of the linearisation, some small differences can be seen between both frequency responses, but still the LPV model captures the launcher dynamics (see right plot in Figure 6).

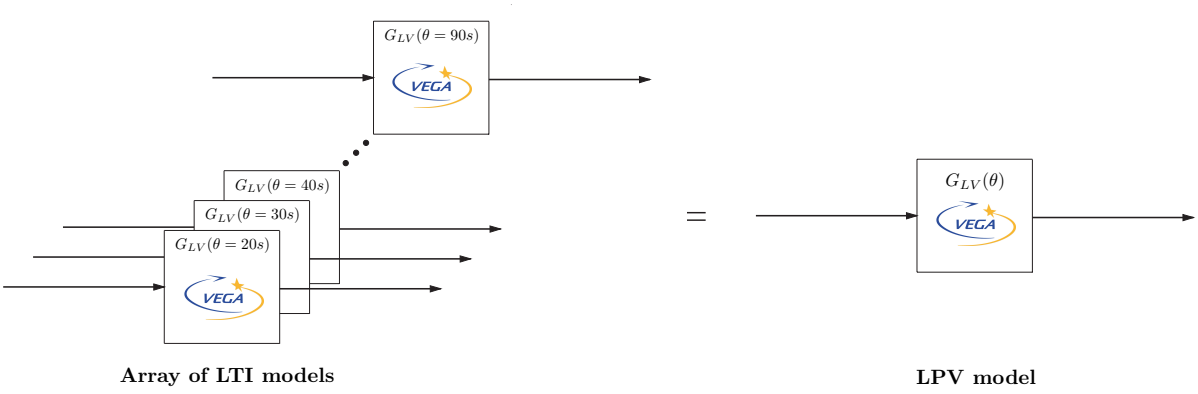

Figure 5: Grid-based LPV modelling approach

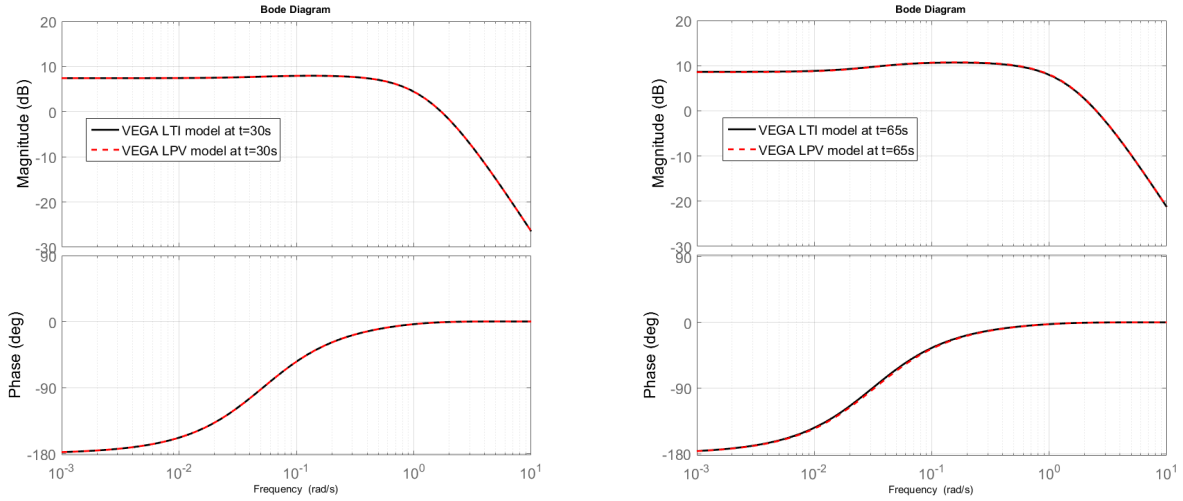

(a) Frequency response ψ_{INS}/β at t=30s

(b) Frequency response ψ_{INS}/β at t=65s

Figure 6: VEGA LPV model validation

4.2 Problem formulation

The LPV controller is also synthesized using the standard $\mathcal{H}_\infty$ interconnection shown in Figure 4. In this case, the VEGA LPV model obtained in the previous section $G_{LV}(\theta)$ is used, generating a generalised plant LPV model $P(\theta)$, which varies as a function of time.

The LPV synthesis is expressed as a linear matrix inequality (LMI) problem, which must be solved to generate a controller. Like $\mathcal{H}_\infty$ theory, the LPV control design relies on weighting functions to impose the desired requirements over the system. The same weighting functions used in subsection 3.2 for the structured $\mathcal{H}_\infty$ design are applied in the LPV design.

The LPV synthesis optimisation consists of finding the controller $K(\theta)$ which minimises the induced $\mathcal{L}_2$ norm of the cost function in equation 31. For a linear time-invariant plant, the induced $\mathcal{L}_2$ norm is equivalent to the $\mathcal{H}_\infty$ norm.

$$\min_{K(\theta)} \|\mathcal{F}_l(M(\theta), K(\theta))\|_\infty \tag{31}$$

where $M(\theta)$ is the augmented LPV closed-loop (including the weighting functions).

The LPV synthesis is also implemented using the MATLAB toolbox LPVTools[8] , through the command *lpvsyn*. This function allows to perform non-rate and rate bounded LPV designs. The former gives the scheduling parameter freedom to vary with infinite parameter rate. This is the simplest LPV design approach, although it may result in conservative designs. On the other hand, the rate bounded design, as the name indicates, limits the rate of the time-varying parameter, but it is more complex.

4.3 LPV design

For ease of simplicity, a non-rate bounded design is performed. The LPV synthesis, like the standard $\mathcal{H}_\infty$ theory, does not define any controller structure. The non-rate bounded LPV controller obtained has 13 states, the same states as the design interconnection of Figure 4. This controller defines a stationary controller for each grid point, and the rest of the controllers are linearly interpolated between the two nearest grid points.

The induced $\mathcal{L}_2$ norm of the synthesized LPV controller is 2.5278. Note that this value is in the range of $\mathcal{H}_\infty$ norms obtained in the structured $\mathcal{H}_\infty$ design. It should be reminded that this result may be conservative, since the controller has to account for every parameter trajectory. This may be improved by using a rate bounded approach. Future work will assess the room for improvement by limiting the scheduling parameter rate for design.

5. Simulation results and discussion

Finally, the structured $\mathcal{H}_\infty$ and LPV designs are implemented and validated in VEGACONTROL, the nonlinear 6 degrees-of-freedom high-fidelity simulator for the VEGA launcher. For further details on this simulator, the reader is referred to.[13] Note that the structured $\mathcal{H}_\infty$ controllers are scheduled using the same controller scheduling rule as for the VEGA baseline control design, as implemented in the VEGACONTROL simulator. The LPV controller is implemented using the Simulink blocks provided in the toolbox LPVTools.[8]

This section compares the baseline controller, the structured $\mathcal{H}_\infty$ and LPV designs. This benchmark is presented in terms of nominal nonlinear time-domain responses and Monte-Carlo simulations. It is highlighted that the verification campaign is not as intensive as that underwent by the baseline, and that this comparison is performed to provide an assessment on the capability to improve the design using more methodological tools and methods.

5.1 Nominal nonlinear time-domain simulation

To evaluate the different controllers, their nominal performance are compared using the VEGACONTROL simulator. Figure 7 shows a comparison of main VEGACONTROL variables (i.e. $Q\alpha$, drift versus altitude, actuation and attitude errors) for the baseline controller (in solid black), the structured $\mathcal{H}_\infty$ design (in dashed blue) and the LPV controller (in dashed-dot green). Since in this work the flexible modes are not considered, the bending modes and the bending filter H_3 have been disabled for this study. In addition, the estimated wind from the VEGA VV05 flight data is injected in the simulator.

Looking at Figure 7a, it can be seen that both robust controllers reduce significantly the aerodynamic loads (approx. 33 % for the structured $\mathcal{H}_\infty$ design and 40 % for the LPV design). This was one of the objectives of the design, to minimise the wind disturbance contribution. The wind generator G_{wind} introduced in the design plays an important role in this task, leading the optimisation to account for real wind levels.

Figure 7b and 7c show the altitude versus drift performance (respectively for the y and z axes). Both robust designs limit the lateral deviation from their respective trajectory with tighter bounds than the baseline controller. This improved performance is achieved even while reducing the TVC deflections around maximum dynamic pressure region (see Figure 7d between t=40s and t=60s) and with a similar attitude error performance (see Figure 7e). However, note that the LPV design presents two higher peaks in the actuation performance with respect to the other controllers in the first 20 seconds of the flight. To avoid this behaviour it may be necessary to increase the range of grid points for the LPV modelling. Recall that the LPV model used in this study only accounts for the interval between t=20s and t=90s.

5.2 Monte-Carlo assessment

To evaluate the robustness, a Monte-Carlo campaign of 1000 runs is performed for the three different controllers assessed in this work. For each run, the same nominal VEGA VV05 flight trajectory is used but set of 125 different operational parameters are dispersed randomly. In VEGACONTROL, an operational parameter can be scattered by means of normalised flags within the range [-1,1], being the zero value the nominal condition. In order to perform a fair comparison, the same scattering flags were used for the three controllers.

Figure 8 shows the 1000 Monte-Carlo time-domain responses for three indicators: the aerodynamic loads, drift performance and attitude errors. Similarly, the baseline controller is depicted in black (see left column), the structured $\mathcal{H}_\infty$ design in blue (middle column) and LPV design in green (right column). From those figures, it can be observed that all the controllers provide good robustness but again the structured $\mathcal{H}_\infty$ and LPV designs can reduce the spread and improve the distance to the safety bounds.

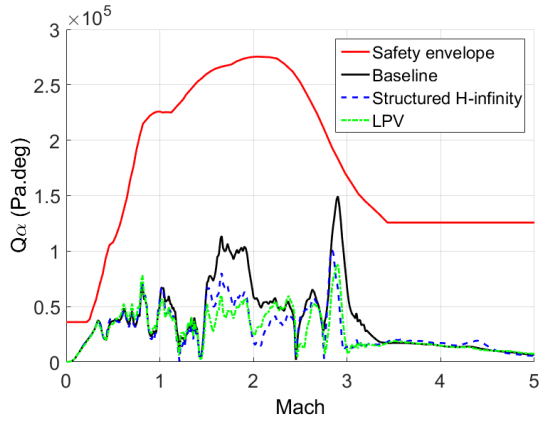

(a) Aerodynamic load

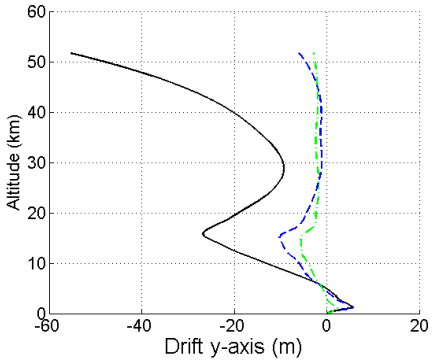

(b) Drift Y-axis vs altitude

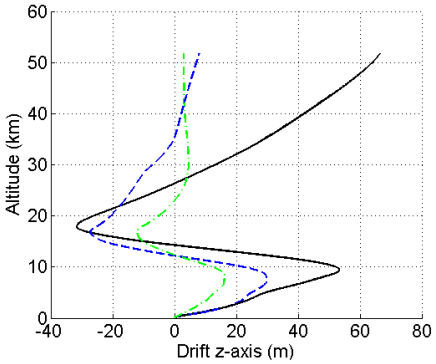

(c) Drift Z-axis vs altitude

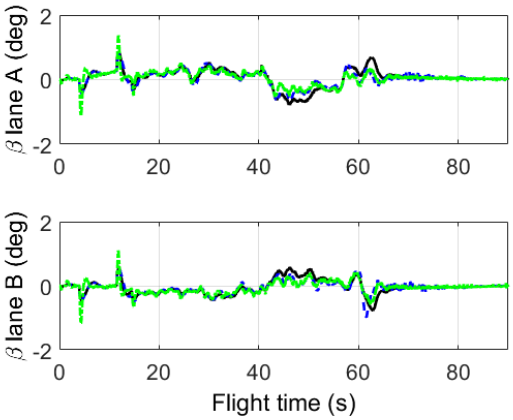

(d) Actuation

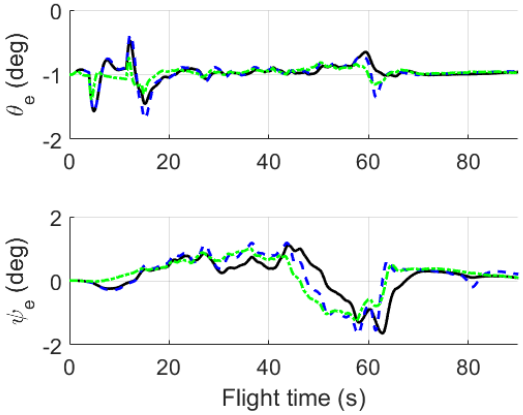

(e) Attitude errors

Figure 7: Nominal nonlinear time-domain responses

Looking at Figure 8a, the baseline controller presents two cases which violate the $Q\alpha$ safety envelope, while the structured $\mathcal{H}_\infty$ design, having the same TVC controller architecture, and the LPV design manage to reduce the loads satisfying the $Q\alpha$ requirement for all the cases. Note that for ease of visualisation there is a change of scale in the y axis between Figure 8d and Figures 8e and 8f.

To quantitative assess the robustness of the three designs, a set of system indicators are evaluated in Table 2. For each indicator and each simulation, two different metrics are considered: the ∞-norm which is equivalent to the maximum value taken by the indicator and the 2-norm, which accounts for the energy of the assessed variable. Table 2 shows the average of those two norms normalised with respect to the baseline controller. For each indicator/norm, the controller which provides better performance is shaded in green.

Comparing the baseline and the structured $\mathcal{H}_\infty$, it can be observed that the latter improves the aerodynamic loads, lateral deviation and actuation indicators at the exchange of presenting slightly worst tracking performance.

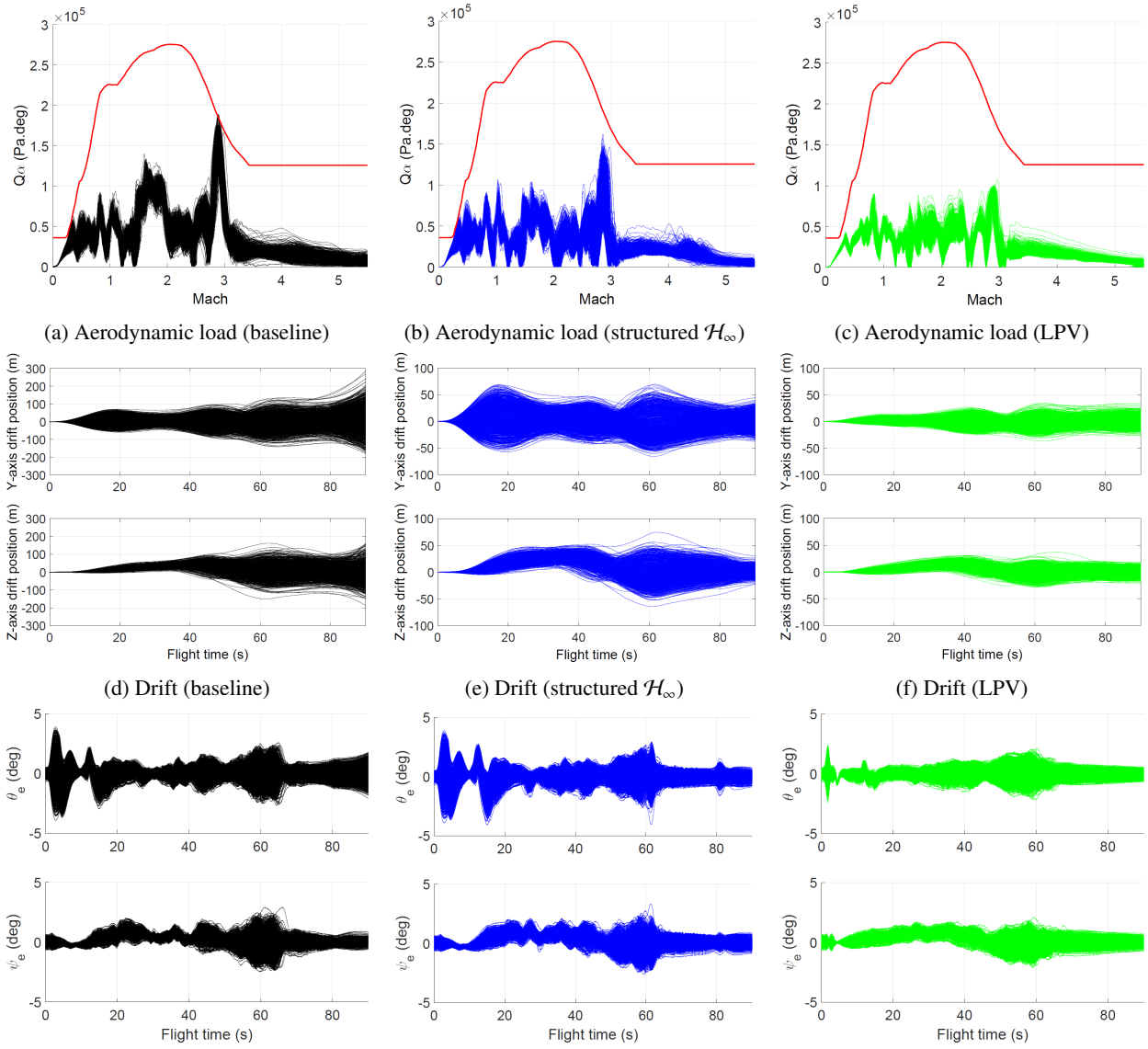

(a) Aerodynamic load (baseline) (b) Aerodynamic load (structured $\mathcal{H}_\infty$) (c) Aerodynamic load (LPV)

(d) Drift (baseline) (e) Drift (structured $\mathcal{H}_\infty$) (f) Drift (LPV)

(g) Attitude errors (baseline) (h) Attitude errors (structured $\mathcal{H}_\infty$) (i) Attitude errors (LPV)

Figure 8: Dispersed Monte-Carlo time-domain responses

Furthermore, the LPV controller offers improved performance for almost all the indicator/norm pairs, except for the ∞-norm of the actuation. This was expected because of the two actuation peaks found in the first 20 seconds of the flight (see Figure 7d). Despite this behaviour, the LPV performance reduces 20 % the actuation energy and therefore TVC consumption.

6. Conclusions

In this work, the structured $\mathcal{H}_\infty$ and LPV synthesis techniques are applied to the design of the rigid-body VEGA launch vehicle attitude control system for the atmospheric phase. Both control designs are addressed using the same standard $\mathcal{H}_\infty$ design interconnection and using the same control objectives, which are expressed in terms of frequency-domain weighting functions. A wind generator based on a wind turbulence Dryden filter is introduced in the design to minimise the wind disturbance contribution in the system. The selection of the set of weighting functions used for design is explained in detail and related to system requirements. In this study, eight linear structured $\mathcal{H}_\infty$ controllers and a non-rate bounded LPV controller are synthesized and implemented in a high-fidelity nonlinear simulator to evaluate and compare their performance and robustness with respect to the baseline controller.

Indicator		Metric	Baseline	Structured $\mathcal{H}_\infty$	LPV
Aerodynamic load	$Q\alpha$	∞-norm	1	0.6785	0.5778
		2-norm	1	0.7713	0.708
Tracking error	y-axis	∞-norm	1	1.0984	0.6142
		2-norm	1	1.05565	0.6642
	z-axis	∞-norm	1	1.1259	0.8398
		2-norm	1	1.1645	1.0219
Actuation	lane A	∞-norm	1	0.9075	1.2584
		2-norm	1	0.8761	0.807
	lane B	∞-norm	1	0.8893	1.2258
		2-norm	1	0.8293	0.8194
Angular rate	p	∞-norm	1	0.9877	1.0584
		2-norm	1	1.0506	0.9537
	q	∞-norm	1	1.035	0.84
		2-norm	1	1.0889	0.8739
Drift	y-axis	∞-norm	1	0.4209	0.1931
		2-norm	1	0.5191	0.223
	z-axis	∞-norm	1	0.49	0.2612
		2-norm	1	0.5527	0.2768
Drift rate	y-axis	∞-norm	1	0.4814	0.2276
		2-norm	1	0.5133	0.2319
	z-axis	∞-norm	1	0.6711	0.3516
		2-norm	1	0.6058	0.3276

Table 2: Monte-Carlo analysis in terms of ∞-norm and 2-norm

The results show that the structured $\mathcal{H}_\infty$ approach can be used to improve the performance and robustness of the system while keeping the same controller structure. Furthermore, the Monte-Carlo simulations exhibit that the LPV controller provides further improved robust performance with respect to the classical and structured $\mathcal{H}_\infty$ designs. These promising results highlight the room for improvement and ease of tuning with these robust methodologies.

Future work is looking at: (i) including the bending filters design in the overall design cycle; (ii) improve the structured $\mathcal{H}_\infty$ robustness by taking into account the system uncertainty in the synthesis stage; and (iii) further study the LPV approach in terms of different modelling and synthesis choices.

7. Acknowledgments

This work was jointly funded by ESA/ELV through the Networking/Partnering Initiative contract No. 4000114460/15/NL/MH/ats. The first author is also the recipient of a Doctoral Training Partnership award by the Engineering and Physical Sciences Research Council (EPSRC).

References

[1] C.D. Andrews. *Terrestrial Environment (Climatic) Criteria Guidelines for Use in Aerospace Vehicle Development*. NASA Technical Memorandum 4511, 1993.

[2] G.J. Balas. Linear, parameter-varying control and its application to a turbofan engine. *International Journal of Robust and Nonlinear Control*, 12:763–796, 2002.

[3] A. Falcoz, C. Pittet, S. Bennani, A. Guignard, C. Bayart, and B. Frapard. Systematic design methods of robust and structured controllers for satellites. *CEAS Space Journal*, 7(3):319–334, 2015.

[4] P. Gahinet and P. Apkarian. Structured $\mathcal{H}_\infty$ Synthesis in MATLAB. In *Proceedings of the* 18^{th} *World Congress of the International Federation of Automatic Control (IFAC)*, volume 18, pages 1435–1440, August 2011.

[5] M. Ganet and M. Ducamp. LPV control for flexible launcher. In *AIAA Guidance, Navigation, and Control Conference*. American Institute of Aeronautics and Astronautics, aug 2010.

[6] M. Ganet-Schoeller. Towards structured $\mathcal{H}_\infty$ synthesis for flexible launcher. In *Proceedings of the* 3^{rd} *CEAS EuroGNC, Specialist Conference on Guidance, Navigation & Control*, April 2015.

[7] A.L. Greensite. *Analysis and Design of Space Vehicle Flight Control Systems. Volume I - Short Period Dynamics*. NASA CR-820, 1967.

[8] A. Hjartarson, P. Seiler, and A. Packard. LPVTools: A toolbox for modeling, analysis, and synthesis of parameter varying control systems. *IFAC-PapersOnLine*, 48(26):139 – 145, 2015.

[9] J. Jang, A. Alaniz, R. Hall, and N. Bedrossian. Ares I flight control system design. In *AIAA Guidance, Navigation, and Control Conference*. American Institute of Aeronautics and Astronautics, aug 2010.

[10] A. Marcos and G.J. Balas. Development of linear-parameter-varying models for aircraft. *Journal of Guidance, Control, and Dynamics*, 27(2):218–228, mar 2004.

[11] A. Marcos and S. Bennani. LPV modeling, analysis and design in space systems: Rationale, objectives and limitations. In *AIAA Guidance, Navigation, and Control Conference*. American Institute of Aeronautics and Astronautics, aug 2009.

[12] A. Marcos and S. Bennani. *A Linear Parameter Varying Controller for a Re-entry Vehicle Benchmark*, pages 15–27. Springer Berlin Heidelberg, Berlin, Heidelberg, 2011.

[13] A. Marcos, P. Rosa, C. Roux, M. Bartolini, and S. Bennani. An overview of the RFCS project V&V framework: optimization-based and linear tools for worst-case search. *CEAS Space Journal*, 7(2):303–318, 2015.

[14] A. Marcos and M. Sato. Flight testing of an structured h-infinity controller: an eu-japan collaborative experience. In *Proceedings of the* 1^{st} *IEEE Conference on Control Technology and Applications (CCTA)*, pages 1590–1595, August 2017.

[15] D. Navarro-Tapia, A. Marcos, S. Bennani, and C. Roux. Structured $\mathcal{H}_\infty$ Control Based on Classical Control Parameters for the VEGA Launch Vehicle. In *Proceedings of the IEEE Conference on Control Applications (CCA)*, September 2016.

[16] D. Navarro-Tapia, A. Marcos, S. Bennani, and C. Roux. Structured h-infinity control design for the VEGA launch vehicle: Recovery of the legacy control behaviour. In *Proceedings of the* 10^{th} *International ESA Conference on Guidance, Navigation and Control Systems (ESA-GNC)*, May 2017.

[17] J. Orr, M. Johnson, J. Wetherbee, and J. McDuffie. State space implementation of linear perturbation dynamics equations for flexible launch vehicles. In *AIAA Guidance, Navigation, and Control Conference*. American Institute of Aeronautics and Astronautics, aug 2009.

[18] C. PitteT and P. Prieur. *Structured Accelero-Stellar Estimator for Microscope Drag-Free Mission*, pages 591–604. Springer International Publishing, 2015.

[19] C. Roux and I. Cruciani. Scheduling schems and control law robustness in atmospheric flight of VEGA. In *Proceedings of the International ESA Conference on Guidance, Navigation and Control Systems*, 2008.

[20] W. J. Rugh and J. S. Shamma. Survey research on gain scheduling. *Automatica*, 36(10):1401–1425, October 2000.

[21] D. Saussié, Q. Barbès, and C. Bérard. Self-Scheduled and Structured H_∞ Synthesis : A Launch Vehicle Application. In *Proceedings of the American Control Conference (ACC)*, pages 1590–1595, June 2013.

[22] P. Simplício, S. Bennani, A. Marcos, C. Roux, and X. Lefort. Structured singular-value analysis of the vega launcher in atmospheric flight. *Journal of Guidance, Control, and Dynamics*, 39(6):1342 – 1355, 2016.

[23] S. Skogestad and I. Postlethwaite. *Multivariable feedback control: analysis and design*. John Wiley & Sons, 2005.

[24] O. Voinot, P. Apkarian, and D. Alazard. Gain-scheduling h-infinity control of the launcher in atmospheric flight via linear-parameter varying techniques. In *AIAA Guidance, Navigation, and Control Conference and Exhibit*. American Institute of Aeronautics and Astronautics, aug 2002.